CHAPTER

11

Nanocomposites based on ethylene vinyl acetate reinforced with different types of nanoparticles: potential applications

Valentina Sessini[1,2], *Marina P. Arrieta*[2], *Alberto Fernández-Torres*[2], *Jean-Marie Raquez*[1], *Philippe Dubois*[1], *José M. Kenny*[3] *and Laura Peponi*[2]

[1]**Laboratory of Polymeric and Composite Materials, University of Mons – UMONS, Mons, Belgium** [2]**Institute of Polymers Science and Technology, ICTP-CSIC, calle Juan de la Cierva 3, Madrid, Spain** [3]**Department of civil and environmental engineering, University of Perugia, Strada di Pentima, Terni, Italy**

11.1 Introduction

Ethylene vinyl acetate (EVA) copolymers are interesting materials for biomedical application such as medical packaging, medical devices, and pharmaceutical applications for over 35 years [1–3].

EVA is a kind of thermoplastic elastomer polymeric material that raises high interest for its easy industrial processing due to the low melting point [4]. The molecular composition of EVA is made of crystalline polyethylene (PE) segments and amorphous poly(vinyl acetate) segments (VA) and therefore EVA exhibits excellent flexibility and shape memory ability [5]. Adjusting the content of VA in the polymer, the material exhibits different microstructural and performance characteristics [4,5].

However, in the biomedical field, EVA applications are limited mainly because their low tensile strength, thermal stability as well as their petrochemical-based origin and nondegradability [6]. Thus to improve its properties, EVA is often used as blends with other polymers [7] or filled

Handbook of Polymer Nanocomposites for Industrial Applications
DOI: https://doi.org/10.1016/B978-0-12-821497-8.00011-3

with nanofillers. The addition of biopolymer component to polyolefin matrices has been widely used to modulate the final properties and reduce the dependence on petrochemical resources by adding a significant biobased component into the polymeric material [7–9]. Moreover, the addition of natural fillers to EVA has proven to be a good option to noticeably increase the stiffness of the resulting material and the strength, especially for low filler content [7,10].

Nanocomposites based on EVA can be potential candidates for several biomedical applications, ranging from medical devices and medical packaging applications, including thermoformed trays, containers, boxes, tubes, needle cover, bottle, blister packs, clamshells, and bottle caps. The formulation of EVA-based nanocomposites that are biostable, easily processable, and with improved mechanical performance is a challenge for the biomedical industry [1]. It is widely known that the incorporation of well-dispersed nanofillers into polymeric matrices can considerably improve a number of specific properties owing to the strong and large polymer/nanofiller interactions [11–13]. Natural inorganic/organic reinforcing materials, such as nanoclay, cellulose, and starch, have gain interest due to their environmental-friendly characteristics [14].

Inorganic fillers have been used to improve the performance of EVA-based materials. Looking at the scientific literature, however, the major results are those based on EVA reinforced with nanoclays and most of the works focus on the investigation of the EVA-based nanocomposites as general film packaging and flame-retardant applications. In 2001 Zanetti et al. reported an interesting work on the thermal behavior of layered silicate-EVA nanocomposites obtained by extrusion [15]. Alexandre et al. [16] studied nanocomposites based on EVA and montmorillonite modified by various alkyl ammonium cations processed by mechanical kneading and they found flame-retardant properties, as well as Beyer [17] who, in 2001, studied the flame-retardant properties of EVA-based nanocomposites indicating that they caused a large decrease in heat release. Alexandre et al. [18] also studied reactive processing to obtain EVA-based nanocomposites. Moreover Riva et al. [19] studied EVA-based nanocomposites for telecommunication cable manufacturing. Bourbigot et al. [20] also studied the design of EVA-based materials for flame retarded low voltage cables and wire. Zanetti et al. [21] studied the combustion behavior of polymer composites based on organically modified phyllosilicates and poly(ethylene-*co*-vinyl acetate) by melt processing. They obtained that the heat release is reduced by 70%–80% when nanocomposites with low silicate loadings (2%–5%) are burned because a protective charred ceramic surface layer is formed as a result of reassembly of the clay layers and catalyzed charring of the polymer. Gelfer et al. [22] investigated a series of nanocomposites prepared by melt-blending of cloisite-based organoclays with poly(ethylene-vinylacetate) (EVA) and neutralized poly(ethylene-methacrylic acid) copolymers and they obtained that the bulk crystallinity is not significantly affected by the presence of organoclays, suggesting that clay particles are predominantly confined in the amorphous phase. Pramanik et al. [23,24] obtained EVA/clay nanocomposites by solution blending, obtaining a delaminated nanocomposites structure with increased mechanical and thermal properties respect to the neat EVA matrix. Zhang et al. [25] studied the effect of both different kinds of clays and different vinyl acetate content on the morphology of EVA-based nanocomposites obtaining not only the intercalated and the exfoliated structure but also they proposed a new nanostructure, "the wedged" to describe the dispersion degree of clay in nanocomposites, it means the sheets of clay were partly wedged by the chains of polymer. Gianelli

et al. [26] in 2004, studied the effect of the processing conditions on EVA-montmorillonite nanocomposites and how its affect the mechanical properties of the final nanocomposites. Pastore et al. [27] found that temperature in the range between 75°C and 350°C, induced structural rearrangements of nanocomposites based on polyethylene-co-vinyl acetate intercalated-organomodified clay (at 3–30 wt.% silicate addition). Chaudary et al. [28] presented a study on different ethylene vinyl acetate (EVA)-based nanocomposites prepared by using EVA with different content of VA (9%, 18%, and 28% VA) filled with different wt.% (2.5, 5, and 7.5) of a montmorillonite-based organomodified clay (Cloisite C15A and C30B) for packaging applications. La Mantia et al. [29] reported a deep study on the rheological behavior of EVA-based nanocomposites. Osman et al. [1,30,31] and Alakrach et al. [32] optimized different formulations of EVA-based nanocomposites for biomedical applications, performing investigations on the structure and properties of the EVA/montmorillonite nanocomposites under ambient and in vitro conditions. They evaluated the biocompatibility and biostability of the obtained materials as part of assessments to determine their suitability for use in a broad range of biomedical applications.

Between natural organic fillers, cellulose derivatives have been widely used in the form of wood and fibers for centuries as reinforcing materials of thermoplastics for the development of composite materials due to cellulose high mechanical properties, low density, inherent biodegradability, and low cost [33–37]. Cellulose is the most abundant polymer in nature, and it is a semicrystalline and high-molecular-weight homopolymer. Nowadays cellulose is exploited in the form of cellulose nanocrystals (CNCs), for the development of nanocomposites in different forms such as films, melt-spun fibers, electrospun fibers, and bulk materials [34,38–42]. High crystalline CNCs can be obtained from several plants and crops, in which they are dissociated from the amorphous parts (composed by hemicellulose and lignin) of cotton and/or wood cellulose fibers under sulfuric acid hydrolysis conditions [34,43]. CNCs have proven to be optimal nanofillers for the development of EVA nanocomposites [43,44]. In this sense, Ma et al. studied EVA rubber/CNCs nanocomposites prepared by solvent casting followed by static vulcanization in the presence of dicumyl peroxide (DCP). A significant reinforcement effect was evidenced by an increase of the tensile strength values approximately 75% and the storage modulus values approximately 50%. Moreover CNCs did not compromise the optical performance and thermal resistance of EVA matrix [44]. Tan et al. developed surface-modified CNCs, by grafting long alkyl chain amine onto carboxylated CNCs, to prepare EVA/CNCs nanocomposite films by means of solvent casting method followed by an orientation process. The amide-based CNCs tensile strength and the elastic modulus drastically increased (~40%), while the typical high elongation of EVA was mainly maintained [43]. The improvement of EVA performance due to development of EVA/CNCs-based nanocomposites was ascribed to the uniform dispersion of the CNCs into the polymeric matrix due to the presence of cross-linker agent [44] or CNCs functionalization [43].

Another polysaccharide studied as nanoreinforcement is starch. Starch represents the major energy reserve of higher plants, it is a mixture of two main components: amylose [a linear or slightly branched (1→4)-α-D-glucan] and amylopectin [a highly branched macromolecule consisting of (1→4)-α-D-glucan short chains linked through α-(1→6) linkages] [45,46]. It is thought that the dominant component of the crystalline region in native starch granules is amylopectin lamellae [45]. Starch can be used as polymeric matrix, in its thermoplastic form [47–50] as well as nanoreinforcing materials in its nanocrystalline form, obtaining starch

nanocrystals (SNCs) [51,52]. However, starch in comparison with cellulose, has been less explored as reinforcing filler due to its large particle size (e.g., several 10 μm) and reduced compatibility with polymer matrix [53]. Accordingly SNCs have gained interest as starch-based reinforcement phase [54]. Among starch botanic sources, SNCs obtained by the hydrolysis of native granules of waxy maize starches have showed special interest because this source is rich in amylopectin (> 99%) [55,56]. SNCs have also proven to be good nanofillers for the development of EVA/SNCs nanocomposites [51,53]. Xu et al. developed EVA/SNCs rubber nanocomposites by using epoxy-functionalized EVA and a silane coupling agent to promote a chemical compatibilization between the nanoreinforcing phase and the polymeric matrix. The cross-linking effect produced a strong reinforcement of EVA matrix, by an increase of the tensile strength values approximately 100% and the storage modulus values approximately 20% [53]. More recently Sessini et al. [51] studied EVA-based nanocomposites reinforced with SNCs obtaining that SNCs do not lose their crystalline nature during the melt processing. The strong hydrogen bonding between SNCs surface and the acetate groups of EVA lead to the improvement of the mechanical and thermal properties of the neat matrix. The elastic modulus values increase approximately 100% adding 5 wt.% of SNCs while the thermal stability increase of approximately 10°C respect to the neat matrix.

In the past years much attention has been focused on multifunctional materials for biomedical applications. Polymers are blended and/or reinforced with nanoparticles to achieve new specific properties, looking for their multifunctionality, biodegradability, and smart behavior [57]. Among smart properties [58] are included self-healing and shape memory, that is, the capability of a polymer to heal itself and the capability of the materials to fix a temporary shape and to recover its initial shape when an external stimulus is applied, respectively. Different are the stimuli that can be applied, temperature, humidity, light, and so on [59]. The most common shape memory effect is due to the temperature. Thus thermally activated shape memory polymers have been designed and synthesized in such a way that two active phases exist in the same material, the fixity phase and the switch phase, having a thermal transition at a determined temperature, named transition temperature (T_{trans}) able to fix the temporary shape as well as to recover the initial shape [60,61].

Regarding EVA-based materials, shape memory is the smart property more studied [62]. EVA-based materials can be designed and processed to show thermally activated shape memory effect using different strategies. Li et al. [63] prepared cross-linked EVA by a two-step method, first dispersing the cross-linking agent (DCP) into the EVA matrix and then cross-linking at elevated temperatures. The shape recovery results indicated that only those specimens that had a sufficiently high cross-linking degree were able to show the shape memory effect. Moreover Nöchel et al. [64] studied the triple-shape capability of cross-linked EVA-based materials programming double temporary shape using two different switching temperatures within the broad melting temperature range of EVA.

In the recent years based on the study of multifunctional response of nanocomposites and in particular on their smart capability, Sessini et al. [47] reported an interesting study on the shape memory behavior of EVA blend and nanocomposites for possible biomedical applications. In particular, when blends of EVA and thermoplastic starch (TPS) were obtained, a double stimuli response has been achieved, the thermal-activated shape memory response due to the presence of EVA and the humidity-activated one due to the presence of starch. The double stimuli response is maintained and improved in the nanocomposites obtained reinforcing the

blends with organoclays. In 2017, Sessini et al. [48] reported a study on the humidity-activated shape memory response increased when natural bentonite is used as reinforcing materials. More recently Sessini et al. [6] studied the thermal and composting degradation of EVA/TPS blends and their nanocomposites reinforced with natural bentonite. Furthermore they reported the compatibilization effect of the bentonite on the immiscible pristine blends.

In the following sections different nanocomposites based on EVA and TPS are presented as example of strategy to obtain EVA-based materials with shape memory properties for potential biomedical applications. In fact, this kind of materials could be used for biomedical applications activating their shape memory effect by mean of only humidity at the human body temperature. In particular EVA/TPS blend was reinforced with different nanofillers such as Cloisite 30B, Cloisite-Na^+, CNCs, and SNCs at 0.5, 1, and 2 wt.%. In comparison with our previous works [47,48], the designing of the nanocomposites was done by one-step method avoiding the preprocessing of the filler with TPS through melt intercalation method. Moreover in this work the effect of different nanofillers on the shape memory response of the nanocomposites has been studied and a different thermally activated shape memory mechanism is proposed.

11.2 Materials and methods

11.2.1 Materials

Native pea starch was obtained from Cosucra groupe Warcoing SA, Belgium, with a dry content of 85 wt.%, including 60.7 wt.% amylopectin, 35.7 wt.% amylose, 3.4 wt.% fiber, and 0.24 wt.% protein, as determined by colorimetric methods and Prosky and DUMAS methods [65]. Starch was used as received. Commercial EVA copolymer (ESCORENE UL00119), with 19 wt.% of vinyl acetate content, was purchase from Exxon Mobil. Glycerol (purity 97%) was purchased from VWR International and it was used as a starch plasticizer. Commercial natural bentonite, Cloisite-Na^+ ($CLNa^+$) and commercial alkyl quaternary ammonium salt bentonite, Cloisite 30B (CL30B), were purchased from BYK Additives and Instruments. Their dimensions are typically ranging from 2 to 13 μm. Microcrystalline cellulose (MCC) and sulfuric acid were purchased from Sigma Aldrich (Spain). Waxy maize starch (N200) used to synthesize the SNCs, was supplied by Roquette Laisa (Spain).

The CNCs were obtained from acid hydrolysis of commercial MCC following a previously reported method [39,42]. In brief an acid hydrolysis was performed using sulfuric acid [64% (wt./wt.)] at 45°C for 30 min under mechanical stirring. To stop the acid hydrolysis, the obtained product was diluted in 4 L of deionized water while the excess of acid was removed by centrifugation. Subsequently the CNCs solution obtained was dialyzed for 5 days to neutralize it. With the aim to purify the solution, an ion exchange resin (Dowex Marathon MR-3 hydrogen and hydroxide form) was added for 24 h to the solution, and it was then removed by filtration. Finally the pH of the solution was adjusted to 9 using a 1.0% NaOH buffer solution to improve the thermal stability of CNCs [66]. Finally the CNCs solution was sonicated to get a stable suspension of the nanofillers. The obtained CNCs exhibit individualized crystal domains with dimensions ranging from 5 to 10 nm in width and from 100 to 200 nm in length, in agreement with previous results [66,67].

SNCs were synthesized by acid hydrolysis as reported in our previous work [49]. In brief waxy maize starch was acid hydrolyzed for 5 days in an aqueous solution of sulfuric acid at 40°C under continuous mechanical stirring (100 rpm). The final suspension was washed by successive centrifugations in distilled water until reaching neutral pH. Finally the solution was filtered and stored at 4°C [51].

11.2.2 Processing of the blends and nanocomposites

Pea starch powder, liquid glycerol, and distilled water were manually premixed 24 h before processing (wt. ratio 100:25:20) to favor the water absorption on the starch granules and their swelling.

The resulting mixture was processed in a Brabender internal kneader at 110°C and 100 rpm for 3 min promoting the destructuration of the crystalline structure of the starch granules and plasticizing the resulting thermoplastic material [48]. Then the nanocomposites were processed mixing in one-step EVA, TPS and the different nanofillers, on a twin-screw DSM microcompounder at 150°C and 125 rpm for 7 min. The composition of the blend were fixed in 60:40 EVA/TPS based on our previous works [47,48].

Melt-processed EVA/TPS nanocomposites were then molded as a thin film by compression-molding at 160°C for 5 min (2 min cooling down the temperature). Nanocomposites reinforced with 0.5, 1, and 2 wt.% of $CLNa^+$, CL30B, CNCs, or SNCs were processed. The compositions of the nanocomposites are given in Table 11.1.

TABLE 11.1 EVA/TPS nanocomposites formulations.

Sample	EVA (%)	TPS (%)	Fillers
EVA/TPS	60	40	0
EVA/TPS/0.5CL30B	59.75	39.75	0.5
EVA/TPS/0.5CLNa^+	59.75	39.75	0.5
EVA/TPS/0.5CNC	59.75	39.75	0.5
EVA/TPS/0.5SNC	59.75	39.75	0.5
EVA/TPS/1CL30B	59.50	39.50	1
EVA/TPS/1CLNa^+	59.50	39.50	1
EVA/TPS/1CNC	59.50	39.50	1
EVA/TPS/1SNC	59.50	39.50	1
EVA/TPS/2CL30B	59	39	2
EVA/TPS/2CLNa^+	59	39	2
EVA/TPS/2CNC	59	39	2
EVA/TPS/2SNC	59	39	2

CL30B, Cloisite 30B; *CLNa*$^+$, Cloisite-Na^+; *CNC*, cellulose nanocrystals; *EVA*, ethylene vinyl acetate; *SNC*, starch nanocrystals; *TPS*, thermoplastic starch.

11.2.3 Characterization methods

The thermal properties were investigated by differential scanning calorimetry (DSC) and thermogravimetric analysis (TGA).

The dynamic DSC measurements were performed in DSC Q200 from TA Instruments, under nitrogen flow (50 mL min^{-1}). Thermal cycles were composed by the following "heat/cool/heat" procedure: heating at 10°C min^{-1} from room temperature to 180°C, cooling at 10°C min^{-1} to −80°C and heating again at 10°C min^{-1} to 180°C. From second and third scans the glass transition temperatures (T_g), the melting temperatures (T_m), the crystallization temperatures (T_c) and the melting enthalpy (ΔH_m) were obtained. The degree of crystallinity (X_c) of each sample was calculated according to the following equation:

$$X_c(\%) = \frac{\Delta H_m}{\Delta H_m^{100}} \times 100 \tag{11.1}$$

where ΔH_m^{100}, is the specific melting enthalpy for a 100% crystalline PE (293 J g^{-1}), considering that VA comonomer units are not able to participate in the crystalline lattice [68].

TGA was conducted using a TA-TGA Q500 thermal analyzer (TA Instruments). Neat EVA and TPS, as well as EVA/TPS blend and its nanocomposites were analyzed by dynamic mode using approximately 10 mg of sample from room temperature to 800°C at 10°C min^{-1} under nitrogen atmosphere with a flow of 60 mL min^{-1}. The initial degradation temperatures ($T_{10\%}$) were calculated at 10% of weight loss and the maximum degradation temperatures (T_{max}) were determined from the first derivative of the TGA curves (DTG).

Dynamic mechanical thermal analysis (DMTA) of the samples was carried out using a DMA Q800 from TA Instruments in film tension mode with an amplitude of 5 μm, a frequency of 1 Hz, a force track of 125%, and a heating rate of 2°C min^{-1}. The samples were cut from compression-molded films into rectangular specimens of approximately 25 mm × 6 mm × 0.50 mm.

Scanning electron microscopy (SEM) micrographs of the cryofracture surface of the blend and its nanocomposites were obtained by SEM (PHILIPS XL30 with a tungsten filament) to study their morphology and the compatibility between EVA and TPS depending on the filler added. The polymer samples were frozen using liquid N_2 and then cryofractured. All the samples were gold/palladium coated by an automatic sputter coated Polaron SC7640. Field emission scanning electron microscope (Hitachi S8000) in transmission mode was used to study the filler dispersion in the nanocomposites.

Thermally activated shape memory properties were studied using a stress-controlled DMA Q800 from TA Instruments in film tension mode. Samples for the thermomechanical cycles were cut from compression-molded films into rectangular specimens of approximately 25 mm × 6 mm × 0.50 mm and characterized using a four-step program. In the 1st step, the samples were kept isothermally at 75°C as switching temperature (T_{sw}), for 5 min, after which the nominal stress was increased with a stress ramp of 0.01 MPa min^{-1}, until 50% of strain. In the 2nd step, the samples were quenched at 10°C (fixing temperature, T_{fix}) for 10 min followed by the 3rd step were the stress was completely unloaded. At this point the temporary shape is programmed. Finally in the 4th step, the samples were heated until the selected T_{sw} at 2°C min^{-1} to activate the free-strain recovery of their permanent shape.

With the aim to get a quantitative estimation of the shape memory properties of the material, the strain fixity ratio (R_f) and the strain recovery ratio (R_r) have been calculated. In particular, R_r, the ability to recover the initial shape, was taken as the ratio of the recovered strain to the total strain, as given by the following equation:

$$R_r(N) = \frac{\varepsilon_m - \varepsilon_p(N)}{\varepsilon_m - \varepsilon_p(N-1)} \times 100 \tag{11.2}$$

R_f, the ability to fix the temporary shape, is the amplitude ratio of the fixed strain to the total strain, as presented by the Eq. (11.2):

$$R_f(N) = \frac{\varepsilon_u(N)}{\varepsilon_m} \times 100 \tag{11.3}$$

where ε_m is the deformed strain, ε_u is the fixed strain, and ε_p is the recovered strain.

A preliminary humidity-activated shape memory test was performed following a procedure previously reported [47]. The samples were conditioned at room temperature and at 80% of RH for 1 week before stretching it until 100% of elongation. Their fixation were performed at room temperature and at 50% of RH while their recovery was triggered in an oven at 37°C and saturated atmosphere [47,69].

11.3 Results and discussion

Fig. 11.1 shows the cryofracture section of the EVA/TPS blend and the nanocomposites reinforced with 2 wt.% of different nanofillers. EVA/TPS blend resulted immiscible. In Fig. 11.1A it is possible to observe nonhomogeneous TPS spherical microdomains dispersed into the rougher EVA matrix [6]. Moreover at higher magnifications (Fig. 11.1B) it is possible to observe phase debonding indicative of the poor adhesion of TPS domains in the polymeric matrix [9,70]. Different morphology was observed for the nanocomposites. In the case of EVA/TPS/2CL30B (Fig. 11.1C), small voids were formed due to TPS debonding from EVA matrix. Nevertheless, it should be mentioned that the TPS domains are smallest and more homogeneous size distribution with respect to that of the EVA/TPS blend indicating the possible improvement of the compatibility between EVA and TPS, due to the addition of the organically modified nanoclay that can have positive interaction with both polymers. Meanwhile in EVA/TPS/2CLNa$^+$ (Fig. 11.1D) no significant changes were observed regarding the size of the microdomains suggesting a probable preferred interaction between the CLNa$^+$ nanoclay and TPS. In the case of the organic fillers, while the addition of CNCs still produce a rougher fracture with debonding TPS microdomains (Fig. 11.1E), the addition of SNCs leads to a flat and homogenous fracture surface without phase separation in which the microdomains practically disappeared (Fig. 11.1F), indicating a good compatibility between SNCs with both polymeric matrices (TPS and EVA).

Dynamic DSC measurements were performed to check the thermal properties and the melt/crystallization behavior of the EVA/TPS blend and its nanocomposites. In Fig. 11.2 the cooling and the second heating scans performed on all materials are represented. No significant changes were observed for the nanocomposites comparing with the neat blend.

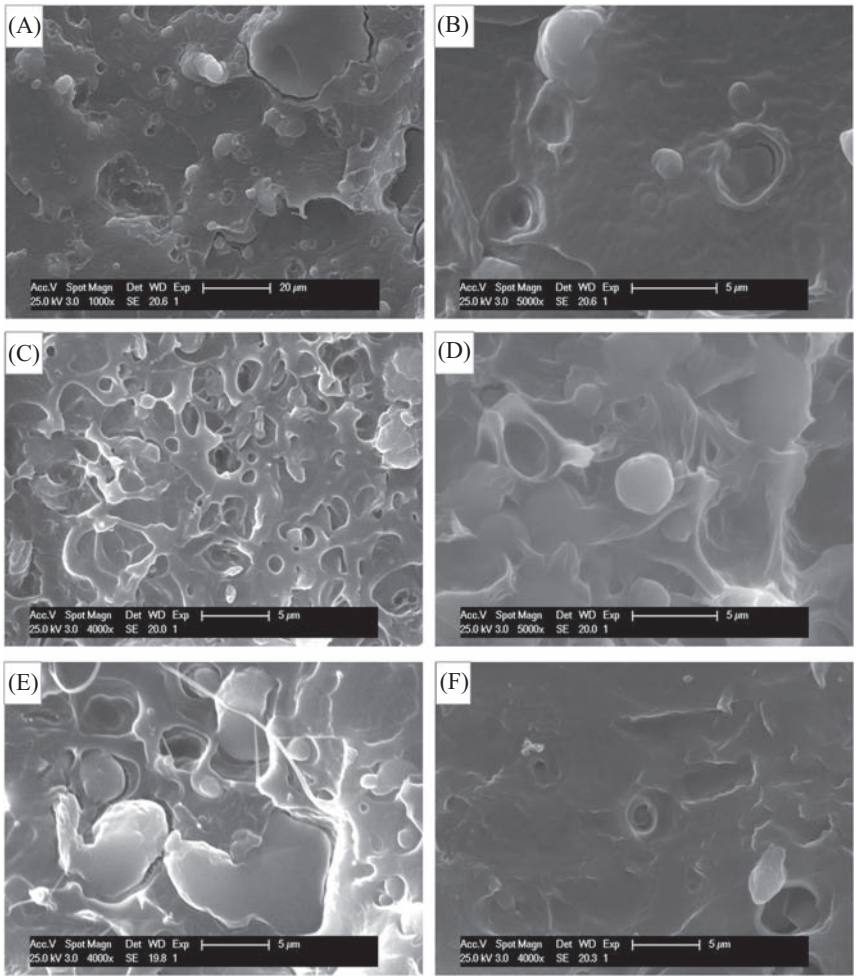

FIGURE 11.1 SEM images of the cryofracture section of the EVA/TPS blend and the nanocomposites: (A) EVA/TPS, (B) EVA/TPS (higher magnification), (C) EVA/TPS/2CL30B, (D) EVA/TPS/2CLNa$^+$, (E) EVA/TPS/2CNC, and (F) EVA/TPS/2SNC. *CL30B*, Cloisite 30B; CLNa$^+$, Cloisite-Na$^+$; *CNC*, cellulose nanocrystals; *EVA*, ethylene vinyl acetate; *SNC*, starch nanocrystals; *TPS*, thermoplastic starch.

All the materials presented the crystallization peak of EVA at 70°C (Fig. 11.2A), the T_g approximately −27°C and the melting peak approximately 85°C. It is worth to note that the thermal transitions of TPS are not clear in the thermograms due to its high dependency on the humidity content [48]. Moreover the melting peak, ascribed to the PE crystal phase of EVA component, is a broad peak that ranges between 30°C and 90°C. As it was demonstrated for copolymers based on PE and methacrylic acid, in our previous work [71], this property allows to thermally activate the shape memory of the material at different switching temperatures within the melting peak.

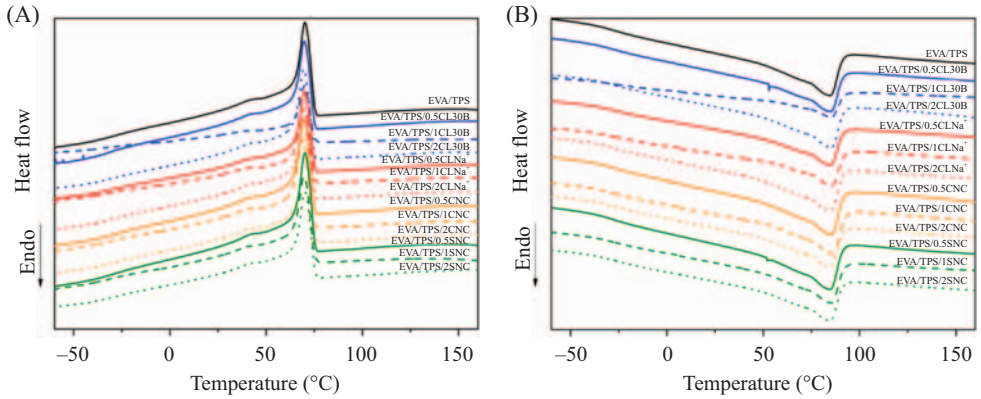

FIGURE 11.2 DSC scans of processed materials: (A) cooling scans and (B) second heating scans. *CL30B*, Cloisite 30B; *CLNa*$^+$, Cloisite-Na$^+$; *CNC*, cellulose nanocrystals; *EVA*, ethylene vinyl acetate; *SNC*, starch nanocrystals; *TPS*, thermoplastic starch.

In Fig. 11.3 the TGA and DTG curves of EVA/TPS blend and the nanocomposites are showed.

Meanwhile, the main thermal parameters obtained from TGA and DTG curves are summarized in Table 11.2. The thermal degradation of EVA/TPS blends takes place in three main steps [6], in which the first one corresponds to TPS degradation [6] and the other two correspond to the degradation of VA groups and to the decomposition of the polyethylenic fraction of EVA, respectively [72]. The TGA curves of EVA/TPS blend and its nanocomposites showed a slightly weight loss from approximately 80°C corresponding to the evaporation of absorbed and bounded water in the films as well as to the loss of low molecular weight compounds (i.e., plasticizer) [6,73].

The TPS addition decreased the onset degradation temperature of EVA approximately 20°C, in good agreement with previous works [73]. On the other side, the TPS thermal stability was improved by the presence of EVA indicating that it is inhibiting the oxidation of the biodegradable matrix during processing [7]. The improvement of the onset thermal degradation of TPS was also observed for all nanocomposites. In fact, all the nanocomposites with 2 wt.% of nanofiller were able to improve the EVA/TPS thermal stability, shifting the onset of the thermal degradation to higher values, between 14°C and 23°C. Meanwhile, lower contents of nanofiller did not increase the thermal stability of the blend. The maximum degradation temperature of TPS was mainly maintained in the blend and nanocomposites. Regarding the EVA decomposition, the thermal degradation process of vinyl acetate takes place in the range of 300°C−390°C, through deacylation with the consequent elimination of acetic acid and the formation of double bonds [74]. All nanocomposites showed somewhat increase of the maximum degradation temperature of VA groups, suggesting a positive interaction between the nanofillers and the carbonyl group of EVA. The CNCs and SNCs, with high amount of −OH groups in their surface, frequently interact with polymeric matrices containing carbonyl groups by hydrogen bonding interactions [44,53,75]. In the case of nanoclays, CL30B was able to considerably increase the T_{max} of VA groups, while CLNa$^+$ showed a similar improvement than organic fillers. In CL30B reinforced materials it

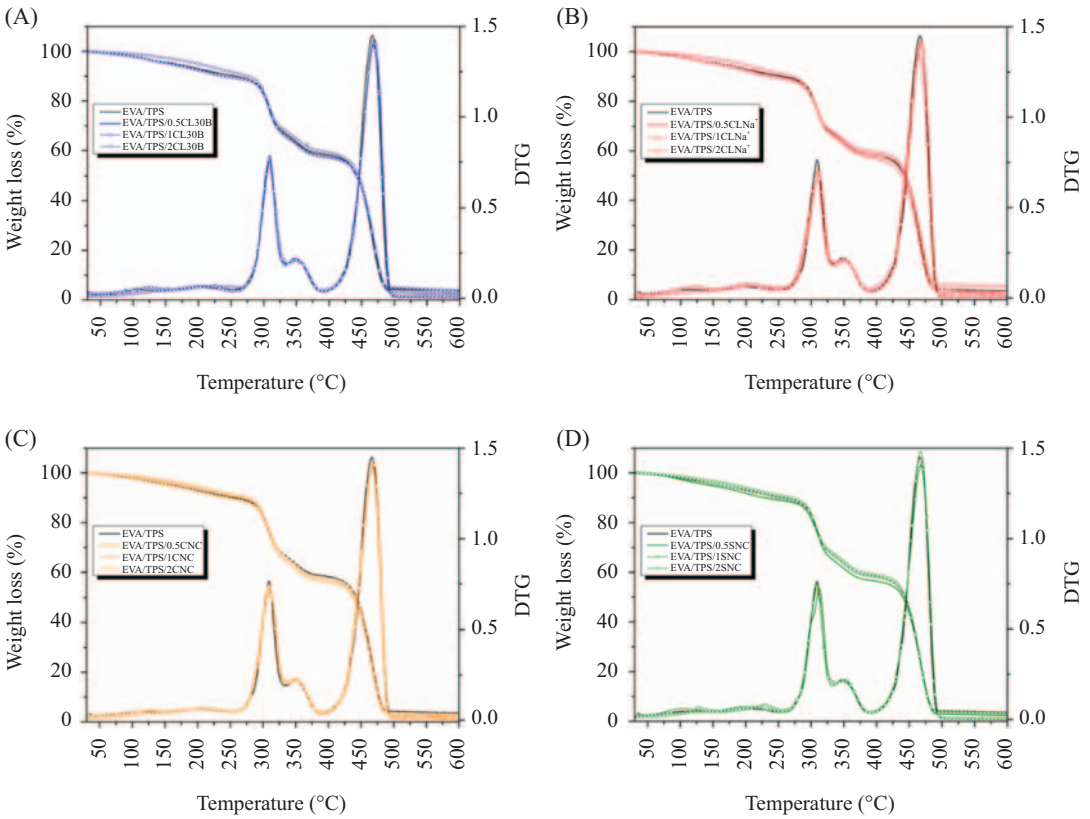

FIGURE 11.3 Thermogravimetric analysis of the processed materials, weight loss profiles, and DTG of the different nanocomposites compared with the neat matrix: (A) CL30B, (B) $CLNa^+$, (C) CNC, and (D) SNC. *CL30B*, Cloisite 30B; *$CLNa^+$*, Cloisite-Na^+; *CNC*, cellulose nanocrystals; *EVA*, ethylene vinyl acetate; *SNC*, starch nanocrystals; *TPS*, thermoplastic starch.

seems that the hydroxyl end groups of alkyl ammonium moieties in the Cloisite layers [76] are interacting with the carbonyl groups of EVA by means of hydrogen bonding interactions, in good agreement with the literature [77]. While unmodified $CLNa^+$ reinforced materials were less able to increase this value because the intercalation of the polymer chains is limited leading to a weak interaction with the polymeric matrix. The T_{max} of PE fraction was mainly maintained, confirming that in these systems the main interactions between starch, EVA, and fillers are established with the vinyl acetate fraction of EVA polymer.

To study the main thermomechanical relaxation of EVA/TPS blend and the nanocomposites and the reinforcing effect of the different fillers, DMTA analysis was performed. The evolution of the storage modulus (E') and damping factor (tan δ) as a function of temperature for the blend and its nanocomposites are presented in Fig. 11.4.

The blend and the different nanocomposites showed the typical relaxations belonging to neat EVA and neat TPS without any shift [48]. The first storage modulus drop corresponds with the glass transition of EVA (β'-relaxation) while the second one is due to the

TABLE 11.2 TGA and DTG thermal properties of neat polymer, EVA/TPS blend and the different nanocomposites.

Sample name	$T_{10\%}$ (°C)	T_{maxTPS} (°C)	T_{maxVA} (°C)	T_{maxPE} (°C)
EVA	356	–	351	465
TPS	203	313	–	–
EVA/TPS	254	309	354	467
EVA/TPS/0.5CL30B	239	309	358	468
EVA/TPS/1CL30B	235	309	360	469
EVA/TPS/2CL30B	276	307	354	470
EVA/TPS/0.5CLNa$^+$	243	311	356	468
EVA/TPS/1CLNa$^+$	234	311	355	465
EVA/TPS/2CLNa$^+$	269	309	355	468
EVA/TPS/0.5CNC	263	309	355	467
EVA/TPS/1CNC	242	309	356	467
EVA/TPS/2CNC	277	309	355	468
EVA/TPS/0.5SNC	227	312	355	468
EVA/TPS/1SNC	247	309	355	468
EVA/TPS/2SNC	271	307	356	468

CL30B, Cloisite 30B; *CLNa$^+$*, Cloisite-Na$^+$; *CNC*, cellulose nanocrystals; *EVA*, ethylene vinyl acetate; *SNC*, starch nanocrystals; *TGA*, thermogravimetric analysis; *TPS*, thermoplastic starch.

melting of PE crystal phase of EVA. It is easy to note that in the case of CLNa$^+$, CNCs, and SNCs-based nanocomposites, the thermodynamic behavior after the glassy/rubbery transition, changed. More likely this is due to the strong interaction between the fillers and the starch-rich phase of the blend, able to shift the β relaxation of starch. Meanwhile, for the CL30B-based nanocomposites any shift was evidenced, even when 2 wt.% of filler was added to the polymeric matrix. This result might confirm the increase of compatibility of EVA and TPS polymers due to the incorporation of organically modified clays that can improve the interaction between polar and apolar components of the blend.

Supporting these results together with the morphological once, the FE-SEM images of CL30B and CLNa$^+$-based nanocomposites with 1 wt.% of nanoclay incorporated are reported in Fig. 11.5.

It is easy to notice, in Fig. 11.5, that CLNa$^+$ have a specific interaction with the TPS polymeric component, being confined preferentially in it. On the contrary, CL30B have interactions with both polymers occupying the interface between EVA and TPS polymeric components and consequently increasing their compatibility, in good accordance with TGA results. Due to the different interactions involved depending on the nature of the nanofillers and their amount in the polymeric matrix, the storage modulus of the nanocomposites did not improve progressively, increasing the nanofillers amount in the blend.

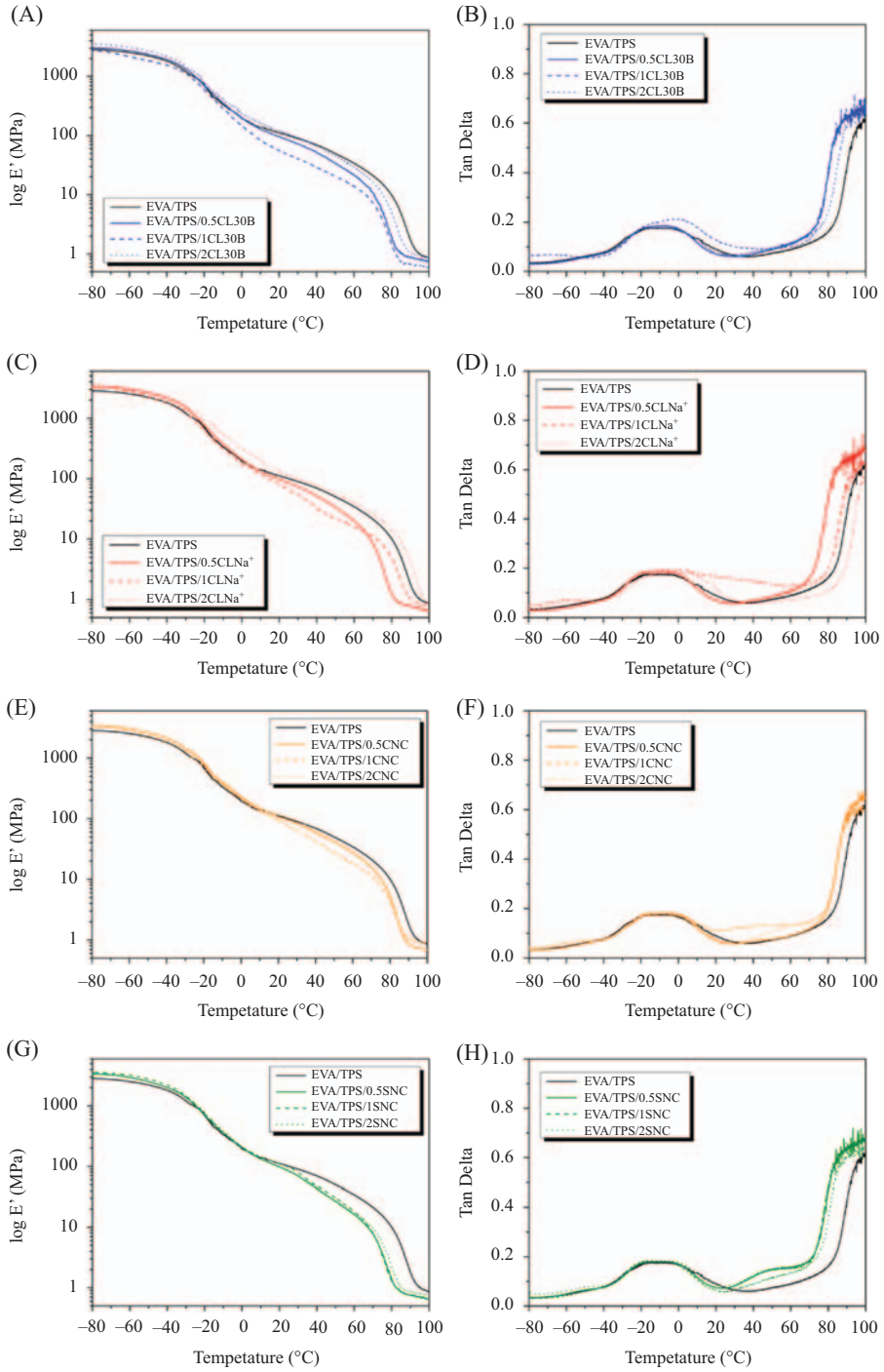

FIGURE 11.4 Dynamic mechanical thermal analysis: (A) and (B) storage modulus and damping factor of the CL30B-based nanocomposites; (C) and (D) storage modulus and damping factor of the $CLNa^+$-based nanocomposites; (E) and (F) storage modulus and damping factor of the CNC-based nanocomposites; (G) and (H) storage modulus and damping factor of the SNC-based nanocomposites. *CL30B*, Cloisite 30B; *$CLNa^+$*, Cloisite-Na^+; *CNC*, cellulose nanocrystals; *EVA*, ethylene vinyl acetate; *SNC*, starch nanocrystals; *TPS*, thermoplastic starch.

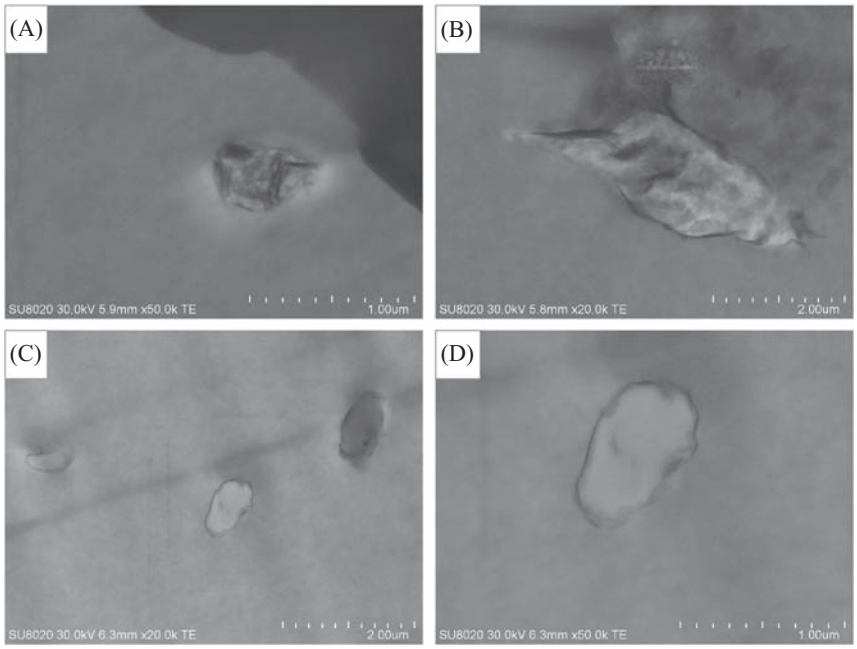

FIGURE 11.5 FE-SEM images of (A) and (B) EVA/TPS/1CLNa$^+$, (C) and (D) EVA/TPS/1CL30B. *CL30B*, Cloisite 30B; *CLNa*$^+$, Cloisite-Na$^+$; *EVA*, ethylene vinyl acetate; *TPS*, thermoplastic starch.

The thermally activated shape memory effect of the materials was studied by proposing a mechanism that consider that the PE crystalline phase of EVA acts as switching phase, fixing the temporary shape and activating the recovering of the permanent one, while TPS together with the remaining biggest PE crystals act as permanent phase able to memorize the permanent shape as well as to store the energy needed for an efficient recovering process. Table 11.3 shows the R_r and R_f values obtained in the thermally activated test for the samples able to perform at least two thermomechanical cycles.

Neat EVA showed very good results in terms of R_r and R_f reaching values higher than 95% for both coefficients. When TPS is added to EVA in the EVA/TPS blend, the stability of the permanent network drastically decreased provoking the breakage of the sample after the second cycle. This behavior is due to the immiscibility between EVA and TPS and to the instability of TPS properties at 75°C, due to the bonded water evaporation. Between all the different nanocomposites the only one able to perform three consecutive thermomechanical cycles was EVA/TPS/1CL30B, reaching maximum values of R_r and R_f of 94 and 99%, respectively.

In Fig. 11.6, an example of humidity-activated shape memory recovery in an oven at 37°C and saturated atmosphere of the samples reinforced with 1 wt.% of fillers is reported. In particular, L_i indicate the initial length of the sample while L_d the deformed length.

The results obtained by the humidity-activated shape memory test are reported in Table 11.4.

TABLE 11.3 Recovery ratio and fixity ratio values of neat blend and the different nanocomposites.

Sample	Cycle	R_r (%)	R_f (%)
EVA	1	77	99
	2	96	98
	3	97	98
EVA/TPS	1	69	99
	2	95	98
EVA/TPS/1CL30B	1	72	99
	2	94	99
	3	94	99
EVA/TPS/1CLNa$^+$	1	67	98
	2	90	100
EVA/TPS/1CNC	1	66	98
	2	79	98

CL30B, Cloisite 30B; *CLNa*$^+$, Cloisite-Na$^+$; *CNC*, cellulose nanocrystals; *EVA*, ethylene vinyl acetate; *TPS*, thermoplastic starch.

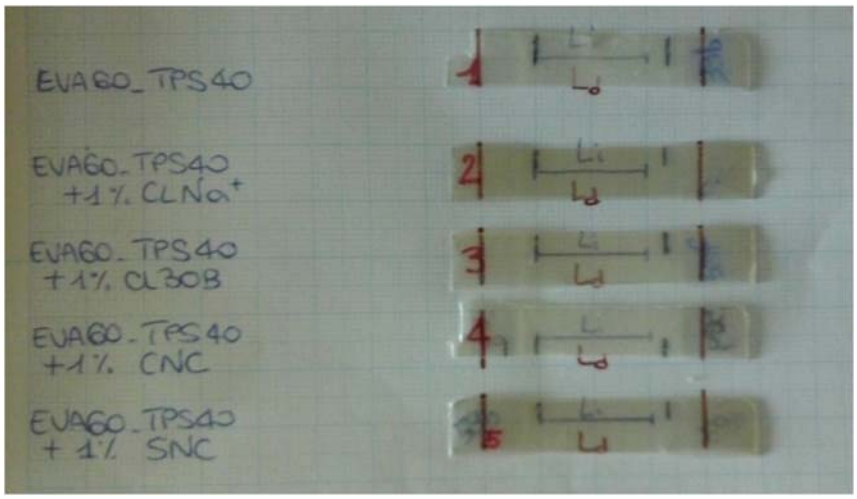

FIGURE 11.6 Humidity-shape memory recovering of the sample filled with 1 wt.% of different fillers.

As it is reported in Table 11.4 an increase of the R_r value in the nanocomposite with 2 wt.% of nanofiller was observed probably due to the hydrophilic behavior of the fillers. The values reflect that the ability to recover the initial shape is good, showing R_r values higher than 70%. Moreover it is easy to notice that during the second cycle the R_f value of the blend drastically decreased while for EVA/TPS/0.5CL30B, EVA/TPS/2CL30B, EVA/

TABLE 11.4 Recovery ratio and fixity ratio values of neat blend and the different nanocomposites.

Sample	Cycle	R_r (%)	R_f (%)
EVA/TPS	1	71	82
	2	75	50
EVA/TPS/0.5CL30B	1	72	59
	2	81	77
EVA/TPS/1CL30B	1	71	82
	2	77	50
EVA/TPS/2CL30B	1	76	66
	2	86	75
EVA/TPS/0.5CLNa$^+$	1	71	56
	2	81	77
EVA/TPS/1CLNa$^+$	1	75	82
	2	82	54
EVA/TPS/2CLNa$^+$	1	75	65
	2	88	68
EVA/TPS/0.5CNC	1	71	66
	2	86	52
EVA/TPS/1CNC	1	68	83
	2	80	60
EVA/TPS/2CNC	1	78	65
	2	87	70
EVA/TPS/0.5SNC	1	74	65
	2	84	56
EVA/TPS/1SNC	1	67	82
	2	80	60
EVA/TPS/2SNC	1	76	63
	2	84	59

CL30B, Cloisite 30B; *CLNa*$^+$, Cloisite-Na$^+$; *CNC*, cellulose nanocrystals; *EVA*, ethylene vinyl acetate; *SNC*, starch nanocrystals; *TPS*, thermoplastic starch.

TPS/0.5CLNa$^+$, EVA/TPS/2CLNa$^+$, EVA/TPS/2CNC, the values are approximately 70% demonstrating that depending on the filled amount, the nanofiller is able to improve the ability to fix the temporary shape. Comparing the results of the humidity-activated shape memory ability with that obtained in our previous works [47,48], we can conclude

that the strain used in the programming step to fix the temporary shape can strongly influence the results in terms of R_r and R_f. In fact, in this work the sample was stretched until 100% while in the past works, the temporary shape was programmed at 50% and 80% of strain. Reaching 100% of strain at 37°C is likely favorizing the crystallization of PE phase of EVA activating the thermally activated shape memory behavior guided by the induced-crystallization mechanism. To obtain better R_r values, in the recovery step the sample should be heated at 60°C to melt the small PE crystals and recover the original shape.

Deep study is needed to optimize the formulation and the design of the EVA-based nanocomposite to improve their humidity-activated shape memory ability as innovative strategy to obtain new materials for potential biomedical applications.

11.4 Conclusions

This chapter focused on polymeric nanocomposite systems based on EVA for potential biomedical applications. A review of the most recent strategies to design and develop EVA-based nanocomposites reinforced with organic and inorganic nanoparticles have been done, highlighting the emerging trends in biomedical nanocomposites and examining new potential fields of application. Moreover different nanocomposites based on EVA were presented as example of strategy to obtain EVA-based materials with shape memory properties for potential biomedical applications. In particular, EVA/TPS blend was reinforced with different nanofillers such as CL30B, $CLNa^+$, CNCs, and SNCs at 0.5, 1, and 2 wt.%. The nanocomposites show shape memory ability and it was found that this property can be affected by the addition of nanoparticles to the neat matrix. TGA results showed that EVA/TPS blends requires the presence of at least 2 wt.% of nanofillers to increase the thermal stability of EVA/TPS blend. TGA also demonstrated that the main interactions in the nanocomposites are between the nanofillers and the VA groups of EVA as well as with TPS. DMTA and morphological results confirm the increase of compatibility between EVA and TPS polymers due to the incorporation of organically modified clays. With the aim to optimize the shape memory ability of EVA-based nanocomposites for potential biomedical applications, deep studies are needed on their processing and design.

Acknowledgments

The authors thank Spanish Ministry of Economy, Industry and Competitiveness, MINEICO (MAT2017-88123-P) for the economic support. L.P. and M.P.A. acknowledge MINEICO for the "Ramon y Cajal" (RYC-2014-15595) and "Juan de la Cierva" (FJCI-2014-20630) contracts. J.M.R. is an FRS-FNRS research associate. J.M.R. and V.S. thank the Wallonia Region, West-Vlaanderen Region, Agentschap Innoveren Ondernemen and European Community (FEDER funds) for the financial support in the frame of the INTERREG V FWVL–BIOHARV project (GoToS3 portofolio).

References

[1] A.F. Osman, A.M. Alakrach, H. Kalo, W.N.W. Azmi, F. Hashim, In vitro biostability and biocompatibility of ethyl vinyl acetate (EVA) nanocomposites for biomedical applications, RSC Adv. 5 (40) (2015) 31485–31495.

[2] R. Healtcare, Pharmaceutical packagingand medical devices. <https://www.repsol.com/imagenes/global/en/repsol_healthcare_catalog_tcm14-58343.pdf>, 2018.

[3] Celanese, Ateva medical eva polymers unique solutions for you. <https://celanese.com/eva-polymers/products/Ateva-G-Medical-Grade.aspx>.
[4] J.R. Subiela, J. López, R. Balart, J.J. García-Jareño, F. Vicente, Electrical properties of EVA filled by zinc powder, J. Mater. Sci. 41 (19) (2006) 6396–6402.
[5] Z.X. Zhang, X.D. Qi, S.T. Li, J.H. Yang, N. Zhang, T. Huang, et al., Water-actuated shape-memory and mechanically-adaptive poly(ethylene vinyl acetate) achieved by adding hydrophilic poly (vinyl alcohol), Eur. Polym. J. 98 (2018) 237–245.
[6] V. Sessini, M.P. Arrieta, J.-M. Raquez, P. Dubois, J.M. Kenny, L. Peponi, Thermal and composting degradation of EVA/Thermoplastic starch blends and their nanocomposites, Polym. Degrad. Stab. 159 (2019) 184–198.
[7] E. Fortunati, D. Puglia, J.M. Kenny, M.M.-U. Haque, M. Pracella, Effect of ethylene-co-vinyl acetate-glycidylmethacrylate and cellulose microfibers on the thermal, rheological and biodegradation properties of poly (lactic acid) based systems, Polym. Degrad. Stab. 98 (12) (2013) 2742–2751.
[8] M.D. Samper, M.P. Arrieta, S. Ferrandiz, J. López, Influence of biodegradable materials in the recycled polystyrene, J. Appl. Polym. Sci. 131 (23) (2014).
[9] M.D. Samper, D. Bertomeu, M.P. Arrieta, J.M. Ferri, J. López-Martínez, Interference of biodegradable plastics in the polypropylene recycling process, Materials 11 (10) (2018).
[10] C.M. Hussain, Handbook of Nanomaterials for Industrial Applications, Elsevier, 2018.
[11] J.M. Raquez, Y. Habibi, M. Murariu, P. Dubois, Polylactide (PLA)-based nanocomposites, Prog. Polym. Sci. 38 (10–11) (2013) 1504–1542.
[12] L. Peponi, D. Puglia, L. Torre, L. Valentini, J.M. Kenny, Processing of nanostructured polymers and advanced polymeric based nanocomposites, Mater. Sci. Eng. R Rep. 85 (2014) 1–46.
[13] C.M. Hussain, Handbook of Functionalized Nanomaterials for Industrial Applications, Elsevier, 2020.
[14] A. Dufresne, J. Castaño, Polysaccharide nanomaterial reinforced starch nanocomposites: a review, Starch-Stärke 69 (1–2) (2017) 1500307.
[15] M. Zanetti, G. Camino, R. Thomann, R. Mülhaupt, Synthesis and thermal behaviour of layered silicate–EVA nanocomposites, Polymer 42 (10) (2001) 4501–4507.
[16] M. Alexandre, G. Beyer, C. Henrist, R. Cloots, A. Rulmont, R. Jérôme, et al., Preparation and properties of layered silicate nanocomposites based on ethylene vinyl acetate copolymers, Macromol. Rapid Commun. 22 (8) (2001) 643–646.
[17] G. Beyer, Flame retardant properties of EVA-nanocomposites and improvements by combination of nanofillers with aluminium trihydrate, Fire Mater. 25 (5) (2001) 193–197.
[18] M. Alexandre, G. Beyer, C. Henrist, R. Cloots, A. Rulmont, R. Jérôme, et al., "One-Pot" preparation of polymer/clay nanocomposites starting from Na + montmorillonite. 1. Melt intercalation of ethylene-vinyl acetate copolymer, Chem. Mater. 13 (11) (2001) 3830–3832.
[19] A. Riva, M. Zanetti, M. Braglia, G. Camino, L. Falqui, Thermal degradation and rheological behaviour of EVA/montmorillonite nanocomposites, Polym. Degrad. Stab. 77 (2) (2002) 299–304.
[20] S. Bourbigot, M. Le Bras, S. Duquesne, M. Rochery, Recent advances for intumescent polymers, Macromol. Mater. Eng. 289 (6) (2004) 499–511.
[21] M. Zanetti, T. Kashiwagi, L. Falqui, G. Camino, Cone calorimeter combustion and gasification studies of polymer layered silicate nanocomposites, Chem. Mater. 14 (2) (2002) 881–887.
[22] M. Gelfer, C. Avila-orta, L. Liu, L. Yang, B. Chu, B.S. Hsiao, et al., Manipulating the microstructure and rheology in polymer-organoclay composites, Polym. Eng. Sci. 42 (9) (2002) 1841–1851.
[23] M. Pramanik, S. Srivastava, B. Samantaray, A. Bhowmick, EVA/clay nanocomposite by solution blending: effect of aluminosilicate layers on mechanical and thermal properties, Macromol. Res. 11 (4) (2003) 260–266.
[24] M. Pramanik, S.K. Srivastava, B.K. Samantaray, A.K. Bhowmick, Rubber–clay nanocomposite by solution blending, J. Appl. Polym. Sci. 87 (14) (2003) 2216–2220.
[25] Wa Zhang, D. Chen, Q. Zhao, Ye Fang, Effects of different kinds of clay and different vinyl acetate content on the morphology and properties of EVA/clay nanocomposites, Polymer 44 (26) (2003) 7953–7961.
[26] W. Gianelli, G. Camino, N.T. Dintcheva, S.L. Verso, F.P.L. Mantia, EVA-montmorillonite nanocomposites: effect of processing conditions, Macromol. Mater. Eng. 289 (3) (2004) 238–244.
[27] H.O. Pastore, A. Frache, E. Boccaleri, L. Marchese, G. Camino, Heat induced structure modifications in polymer-layered silicate nanocomposites, Macromol. Mater. Eng. 289 (9) (2004) 783–786.

[28] D. Chaudhary, R. Prasad, R. Gupta, S. Bhattacharya, Clay intercalation and influence on crystallinity of EVA-based clay nanocomposites, Thermochim. Acta 433 (1–2) (2005) 187–195.
[29] F. La Mantia, N.T. Dintcheva, Eva copolymer-based nanocomposites: rheological behavior under shear and isothermal and non-isothermal elongational flow, Polym. Test. 25 (5) (2006) 701–708.
[30] A.F. Osman, H. Kalo, M.S. Hassan, T.W. Hong, F. Azmi, Pre-dispersing of montmorillonite nanofiller: impact on morphology and performance of melt compounded ethyl vinyl acetate nanocomposites, J. Appl. Polym. Sci. 133 (11) (2016).
[31] A.F. Osman, T.F.M. Fitri, M. Rakibuddin, F. Hashim, S.A.T. Tuan Johari, R. Ananthakrishnan, et al., Pre-dispersed organo-montmorillonite (organo-MMT) nanofiller: morphology, cytocompatibility and impact on flexibility, toughness and biostability of biomedical ethyl vinyl acetate (EVA) copolymer, Mater. Sci. Eng. C 74 (2017) 194–206.
[32] A.M. Alakrach, A.F. Osman, N.Z. Noriman, B.O. Betar, O.S. Dahham, Thermal properties of ethyl vinyl acetate (EVA)/montmorillonite (MMT) nanocomposites for biomedical applications, MATEC Web Conf. 78 (2016).
[33] E. Rayón, S. Ferrandiz, M.I. Rico, J. López, M.P. Arrieta, Microstructure, mechanical, and thermogravimetric characterization of cellulosic by-products obtained from biomass seeds, Int. J. Food Prop. 18 (6) (2015) 1211–1222.
[34] L. Brinchi, F. Cotana, E. Fortunati, J. Kenny, Production of nanocrystalline cellulose from lignocellulosic biomass: technology and applications, Carbohydr. Polym. 94 (1) (2013) 154–169.
[35] L. Peponi, J. Biagiotti, L. Torre, J.M. Kenny, I. Mondragòn, Statistical analysis of the mechanical properties of natural fibers and their composite materials. I. Natural fibers, Polym. Compos. 29 (3) (2008) 313–320.
[36] L. Peponi, J. Biagiotti, J.M. Kenny, I. Mondragon, Statistical analysis of the mechanical properties of natural fibers and their composite materials. II. Composite materials, Polym. Compos. 29 (3) (2008) 321–325.
[37] G. Lo, Re, V. Sessini, Wet feeding approach for cellulosic materials/PCL biocomposites, ACS Symp. Ser. (2018) 209–226.
[38] M.P. Arrieta, E. Fortunati, N. Burgos, M.A. Peltzer, J. López, L. Peponi, Nanocellulose-based polymeric blends for food packaging applications, Multifunctional Polymeric Nanocomposites Based on Cellulosic Reinforcements, 2016, pp. 205–252.
[39] I. Navarro-Baena, J.M. Kenny, L. Peponi, Thermally-activated shape memory behaviour of bionanocomposites reinforced with cellulose nanocrystals, Cellulose 21 (6) (2014) 4231–4246.
[40] A. Mujica-Garcia, S. Hooshmand, M. Skrifvars, J.M. Kenny, K. Oksman, L. Peponi, Poly (lactic acid) melt-spun fibers reinforced with functionalized cellulose nanocrystals, RSC Adv. 6 (11) (2016) 9221–9231.
[41] Á. Sonseca, S. Camarero-Espinosa, L. Peponi, C. Weder, E.J. Foster, J.M. Kenny, et al., Mechanical and shape-memory properties of poly (mannitol sebacate)/cellulose nanocrystal nanocomposites, J. Polym. Sci. Part. A: Polym. Chem. 52 (21) (2014) 3123–3133.
[42] V. Sessini, I. Navarro-Baena, M.P. Arrieta, F. Dominici, D. López, L. Torre, et al., Effect of the addition of polyester-grafted-cellulose nanocrystals on the shape memory properties of biodegradable PLA/PCL nanocomposites, Polym. Degrad. Stab. 152 (2018) 126–138.
[43] C. Tan, J. Peng, W. Lin, Y. Xing, K. Xu, J. Wu, et al., Role of surface modification and mechanical orientation on property enhancement of cellulose nanocrystals/polymer nanocomposites, Eur. Polym. J. 62 (2015) 186–197.
[44] P. Ma, L. Jiang, M. Hoch, W. Dong, M. Chen, Reinforcement of transparent ethylene-co-vinyl acetate rubber by nanocrystalline cellulose, Eur. Polym. J. 66 (2015) 47–56.
[45] N. Lin, J. Huang, P.R. Chang, D.P. Anderson, J. Yu, Preparation, modification, and application of starch nanocrystals in nanomaterials: a review, J. Nanomater. (2011)(2011) 20.
[46] D. Lu, C. Xiao, S. Xu, Starch-based completely biodegradable polymer materials, Express Polym. Lett. 3 (6) (2009) 366–375.
[47] V. Sessini, J.-M. Raquez, G. Lo Re, R. Mincheva, J.M. Kenny, P. Dubois, et al., Multiresponsive shape memory blends and nanocomposites based on starch, ACS Appl. Mater. Interfaces 8 (30) (2016) 19197–19201.
[48] V. Sessini, J.-M. Raquez, D. Lourdin, J.-E. Maigret, J.M. Kenny, P. Dubois, et al., Humidity-activated shape memory effects on thermoplastic starch/EVA blends and their compatibilized nanocomposites, Macromol. Chem. Phys. 218 (24) (2017) 1700388.
[49] V. Sessini, M.P. Arrieta, J.M. Kenny, L. Peponi, Processing of edible films based on nanoreinforced gelatinized starch, Polym. Degrad. Stab. 132 (2016) 157–168.

[50] J. Li, M. Zhou, G. Cheng, F. Cheng, Y. Lin, P.-X. Zhu, Fabrication and characterization of starch-based nanocomposites reinforced with montmorillonite and cellulose nanofibers, Carbohydr. Polym. 210 (2019) 429–436.
[51] V. Sessini, J.-M. Raquez, J.M. Kenny, P. Dubois, L. Peponi, Melt-processing of bionanocomposites based on ethylene-co-vinyl acetate and starch nanocrystals, Carbohydr. Polym. 208 (2019) 382–390.
[52] V. Sessini, M.P. Arrieta, A. Fernández-Torres, L. Peponi, Humidity-activated shape memory effect on plasticized starch-based biomaterials, Carbohydr. Polym. 179 (2018) 93–99.
[53] P. Xu, X. Zhao, P. Ma, M. Chen, W. Dong, M. Hoch, et al., Design of nano-starch-reinforced ethyl-co-vinyl acetate elastomers by simultaneously constructing interfacial bonding and novel reversible matrix crosslinking, Chem. Eng. J. 346 (2018) 497–505.
[54] D. Le Corre, J. Bras, A. Dufresne, Starch nanoparticles: a review, Biomacromolecules 11 (5) (2010) 1139–1153.
[55] D. Le Corre, H. Angellier-Coussy, Preparation and application of starch nanoparticles for nanocomposites: a review, React. Funct. Polym. 85 (2014) 97–120.
[56] D. LeCorre, J. Bras, A. Dufresne, Influence of botanic origin and amylose content on the morphology of starch nanocrystals, J. Nanopart. Res. 13 (12) (2011) 7193–7208.
[57] F. Pilate, A. Toncheva, P. Dubois, J.-M. Raquez, Shape-memory polymers for multiple applications in the materials world, Eur. Polym. J. 80 (2016) 268–294.
[58] L. Peponi, M. Arrieta, A. Mujica-Garcia, D. López, Smart Polymers, Modification of Polymer Properties, Elsevier, 2017, pp. 131–154.
[59] V. Sessini, J.M. Raquez, P. Dubois, J.M. Kenny, L. Peponi, Stimuli-responsive polymeric materials with shape memory ability, in: L. Peponi, J.-M. Raquez (Eds.), How Smart are the Polymers? NOVA Science Publishers, 2018, pp. 1–33.
[60] L. Peponi, I. Navarro-Baena, J. Kenny, Shape Memory Polymers: Properties, Synthesis and Applications, Smart Polymers and their Applications, Elsevier, 2014, pp. 204–236.
[61] M.P. Arrieta, V. Sessini, L. Peponi, Biodegradable poly(ester-urethane) incorporated with catechin with shape memory and antioxidant activity for food packaging, Eur. Polym. J. 94 (2017) 111–124.
[62] B.P. Federation, Shape memory polymers—a complete guide. <https://www.bpf.co.uk/plastipedia/applications/shape-memory-polymer.aspx>.
[63] F. Li, W. Zhu, X. Zhang, C. Zhao, M. Xu, Shape memory effect of ethylene–vinyl acetate copolymers, J. Appl. Polym. Sci. 71 (7) (1999) 1063–1070.
[64] U. Nöchel, U.N. Kumar, K. Wang, K. Kratz, M. Behl, A. Lendlein, Triple-shape effect with adjustable switching temperatures in crosslinked poly[ethylene-co-(vinyl acetate)], Macromol. Chem. Phys. 215 (24) (2014) 2446–2456.
[65] J.M. Raquez, A. Bourgeois, H. Jacobs, P. Degée, M. Alexandre, P. Dubois, Oxidative degradations of oxodegradable LDPE enhanced with thermoplastic pea starch: thermo-mechanical properties, morphology, and UV-ageing studies, J. Appl. Polym. Sci. 122 (1) (2011) 489–496.
[66] E. Fortunati, I. Armentano, Q. Zhou, A. Iannoni, E. Saino, L. Visai, et al., Multifunctional bionanocomposite films of poly (lactic acid), cellulose nanocrystals and silver nanoparticles, Carbohydr. Polym. 87 (2) (2012) 1596–1605.
[67] M.P. Arrieta, E. Fortunati, F. Dominici, E. Rayón, J. López, J.M. Kenny, Multifunctional PLA–PHB/cellulose nanocrystal films: processing, structural and thermal properties, Carbohydr. Polym. 107 (2014) 16–24.
[68] M. Brogly, M. Nardin, J. Schultz, Effect of vinylacetate content on crystallinity and second-order transitions in ethylene—vinylacetate copolymers, J. Appl. Polym. Sci. 64 (10) (1997) 1903–1912.
[69] J. Mendez, P.K. Annamalai, S.J. Eichhorn, R. Rusli, S.J. Rowan, E.J. Foster, et al., Bioinspired mechanically adaptive polymer nanocomposites with water-activated shape-memory effect, Macromolecules 44 (17) (2011) 6827–6835.
[70] M. Aldas, J.M. Ferri, J. Lopez-Martinez, M.D. Samper, M.P. Arrieta, Effect of pine resin derivatives on the structural, thermal, and mechanical properties of mater-bi type bioplastic, J. Appl. Polym. Sci. (2019).
[71] V. Sessini, D. Brox, A.J. López, A. Ureña, L. Peponi, Thermally activated shape memory behavior of copolymers based on ethylene reinforced with silica nanoparticles, Nanocomposites 4 (2) (2018) 19–35.
[72] M. Pracella, M.M.U. Haque, V. Alvarez, Compatibilization and properties of EVA copolymers containing surface-functionalized cellulose microfibers, Macromol. Mater. Eng. 295 (10) (2010) 949–957.

[73] A.L. Da Róz, A.M. Ferreira, F.M. Yamaji, A.J.F. Carvalho, Compatible blends of thermoplastic starch and hydrolyzed ethylene-vinyl acetate copolymers, Carbohydr. Polym. 90 (1) (2012) 34–40.
[74] D. Nguyen, T. Vu, A.-C. Grillet, H.H. Thuc, C.H. Thuc, Effect of organoclay on morphology and properties of linear low density polyethylene and Vietnamese cassava starch biobased blend, Carbohydr. Polym. 136 (2016) 163–170.
[75] M.P. Arrieta, J. López, D. López, J.M. Kenny, L. Peponi, Biodegradable electrospun bionanocomposite fibers based on plasticized PLA–PHB blends reinforced with cellulose nanocrystals, Ind. Crop. Prod. 93 (2016) 290–301.
[76] C. Villegas, M.P. Arrieta, A. Rojas, A. Torres, S. Faba, M.J. Toledo, et al., PLA/organoclay bionanocomposites impregnated with thymol and cinnamaldehyde by supercritical impregnation for active and sustainable food packaging, Compos. Part. B: Eng. 176 (2019) 107336.
[77] X. Li, C.S. Ha, Nanostructure of EVA/organoclay nanocomposites: effects of kinds of organoclays and grafting of maleic anhydride onto EVA, J. Appl. Polym. Sci. 87 (12) (2003) 1901–1909.